Antiproliferative properties of iron supramolecular cylinders

Rosa F. Brissos [a], Luís Korrodi-Gregório [b], Ricardo Pérez-Tomás [b], Olivier Roubeau [c], Patrick Gamez [a,d,e*].

Email: patrick.gamez@qi.ub.es

[a] Department of Inorganic and Organic Chemistry, Inorganic Chemistry Section, University of Barcelona, Martí i Franquès 1-11, 08028 Barcelona, Spain.
[b] Department of Pathology and Experimental Therapeutics, Faculty of Medicine, University of Barcelona, Campus Bellvitge, Feixa Llarga s/n, 08907 L'Hospitalet de Llobregat, Spain.
[c] Instituto de Ciencia de Materiales de Aragón, CSIC and Universidad de Zaragoza, Plaza San Francisco s/n, 50009 Zaragoza, Spain.
[d] Catalan Institution for Research and Advanced Studies, Passeig Lluís Companys 23, 08010 Barcelona, Spain.
[e] Institute of Nanoscience and Nanotechnology, Martí i Franquès 1-11, 08028 Barcelona, Spain.

Supporting Information

Table of Contents

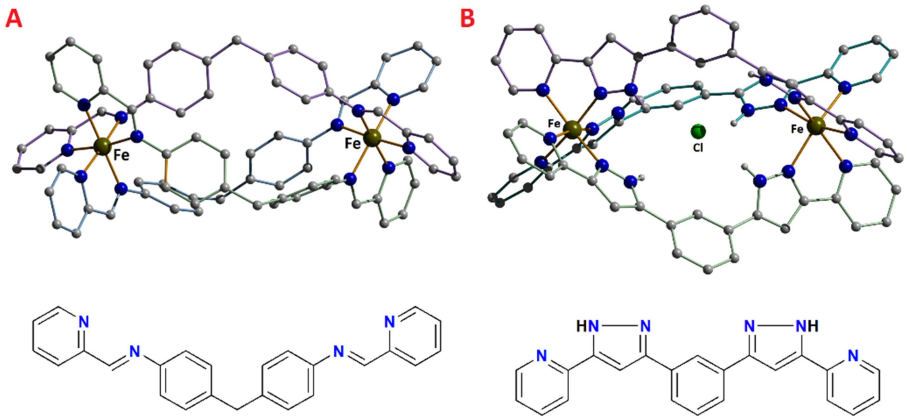

Figure S1. Representation of the crystal structures (cationic part) of known iron-based helicates together with their corresponding ligand, which were used in the present study for comparison purposes. A) $[Fe_2(C_{25}H_{20}N_4)_3]Cl_4$ (**R1**) [1] and B) $Cl@[Fe_2(C_{22}H_{16}N_6)_3]Cl(PF_6)_2$ (**R2**) [2].

Table S1. Crystal data and structure refinement for metallohelicates **H1** and **H2**.

Compound	**H1**	**H2**
Empirical formula	$C_{99}H_{65}Fe_2NO_{12.25}$	$C_{76}H_{58}Fe_2N_2O_{20}$
Formula weight (g mol^{-1})	1576.22	1430.94
Temperature (K)	100(2)	100(2)
Crystal system	triclinic	monoclinic
Space group	*P*−1	*C*2/c
Crystal size (mm^3)	0.20 × 0.04 × 0.03	0.06 × 0.02 × 0.01
a (Å)	15.300(2)	23.016(4)
b (Å)	16.940(3)	17.915(3)
c (Å)	17.496(3)	18.590(6)
a (°)	64.285(2)	90
β (°)	72.373(2)	121.900(2)
γ (°)	82.106(2)	90
V (Å^3)	3893.6(11)	6508(3)
Z	2	4
ϱ_{calcd}	1.344	1.461
μ (mm^{-1})	0.551	0.661
F(000)	1632	2960
θ for data collection (°)	2.85− 26.22	2.71− 33.17
Reflections collected / unique	56858 / 11975	32347 / 8404
Completeness to theta	0.991	0.998
Data / restraints / parameters	11975/ 586 / 1161	8404 / 112 / 495
Goodness-of-fit on F^2	1.074	1.034
Final *R* indices [$I>2\sigma(I)$]	R1 = 0.0815, wR2 = 0.1960	R1 = 0.0601, wR2 = 0.1524
R indices (all data)	R1 = 0.1263, wR2 = 0.2245	R1 = 0.1022, wR2 = 0.1743
largest diff. peak and hole (*e* Å^3)	0.713 and −0.407	1.162 and −0.570

Table S2. Selected bond lengths (Å) and angles (°) for metallohelicates **H1** and **H2**.

H1			
Fe1−O1	2.018(5)	Fe1−O2	2.001(5)
Fe1−O5	1.975(4)	Fe1−O6	2.000(4)
Fe1−O9	1.980(4)	Fe1−O10	1.966(4)
Fe2−O3	1.977(5)	Fe2−O4	1.987(5)
Fe2−O7	1.977(5)	Fe2−O8	1.979(6)
Fe2−O11	1.982(4)	Fe2−O12	1.970(5)
O1−Fe1−O2	85.64(19)	O2−Fe1−O6	83.60(18)
O6−Fe1−O9	97.38(18)	O9−Fe1−O1	94.25(18)
O2−Fe1−O5	97.48(18)	O5−Fe1−O9	88.63(18)
O9−Fe1−O10	86.05(17)	O10−Fe1−O2	87.93(17)
O3−Fe2−O4	87.0(2)	O4−Fe2−O8	87.6(2)
O8−Fe2−O11	97.1(2)	O11−Fe2−O3	88.69(18)
O4−Fe2−O7	95.80(19)	O7−Fe2−O11	86.95(17)
O11−Fe2−O12	86.88(18)	O12−Fe2−O4	90.7(2)
H2			
Fe1−O2	1.969(2)	Fe1−O3	1.966(3)
Fe1−O8	2.010(2)	Fe1−O9	1.973(2)
Fe1−O4a[a]	2.021(2)	Fe1−O5a[a]	2.008(3)
O2−Fe1−O3	86.75(10)	O3−Fe1−O9	87.30(10)
O9−Fe1−O5a	100.21(11)	O5a−Fe1−O2	86.64(10)
O3−Fe1−O4a	86.81(10)	O4a−Fe1−O5a	84.97(10)
O5a−Fe1−O8	91.41(11)	O8−Fe1−O3	97.90(10)

[a]Symmetry operation: a = 1−x, y, 1/2−z.

Table S3. Selected contact distances (Å) for metallohelicates **H1** and **H2**.

H1	π−π interactions	
C58B···C64Bf	3.383(18)	
centroid···centroid	3.712(2)	
H2	Hydrogen bonds and π−π interactions	
O1−H1···O4	2.748(4)	165(5)
O6a[a]−H6a···O1w	2.611(15)	164
O7−H7···N1s	2.756(6)	152(4)
C1···C7	3.326(8)	

[a]Symmetry operation: a = 1−x, y, 1/2−z, 1+z; f = 1−x, −y, 2−z

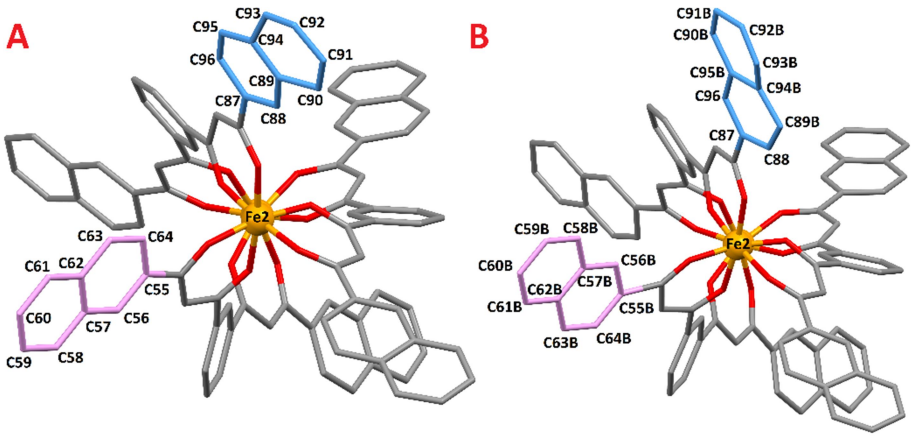

Figure S2. Major (60%) and minor (40%) conformations of **H1** present in the crystal lattice.

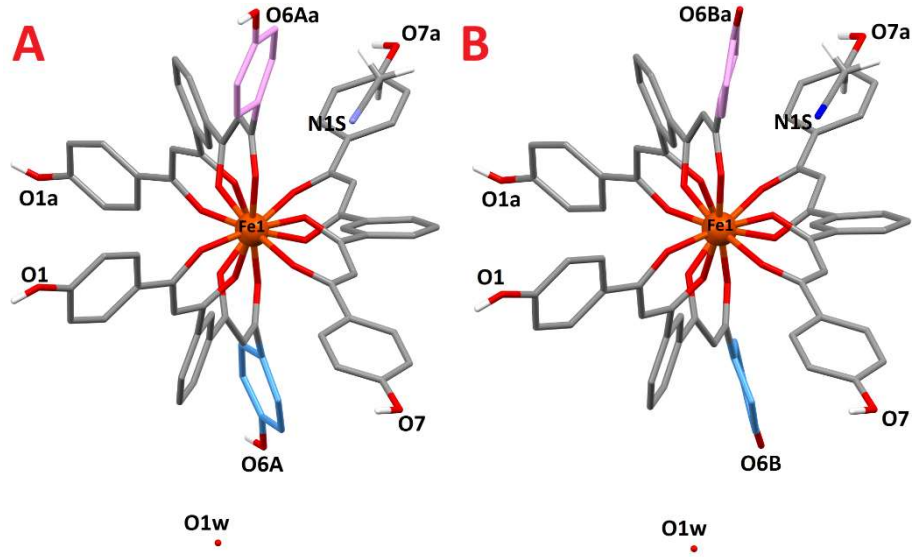

Figure S3. Major (60%) and minor (40%) conformations of **H2** present in the crystal lattice.

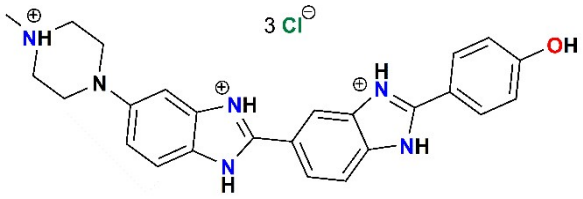

Figure S4. Representation of Hoechst 33258 (2'-(4-hydroxyphenyl)-5-(4-methyl-1-piperazinyl)-2,5'-bi-1*H*-benzimidazole trihydrochloride hydrate).

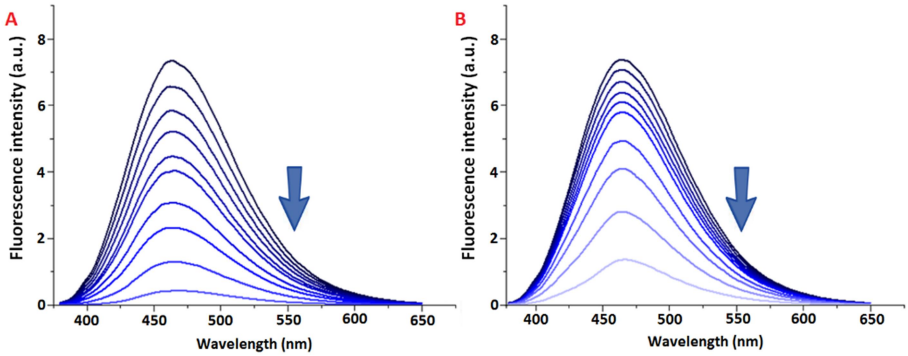

Figure S5. Emission spectra of DNA-Hoechst complex ([DNA] = 0.19 μM and [Hoechst 33258] = 15 μM), λ_{exc} = 349 nm, λ_{em} = 458 nm, upon addition of increasing amounts (2–150 μM) of A) **H1** and B) **H2**. The blue arrows show the diminution of the emission intensity with the increase of the complex concentration.

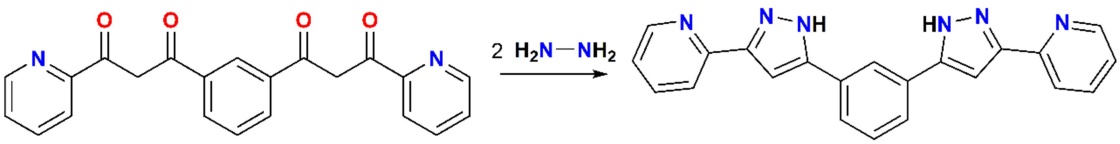

Figure S6. Preparation of the ligand found in Cl@[$Fe_2(C_{22}H_{16}N_6)_3$]Cl(PF_6)$_2$ (**R2**), which is obtained from a bis-β-diketone and hydrazine [2].

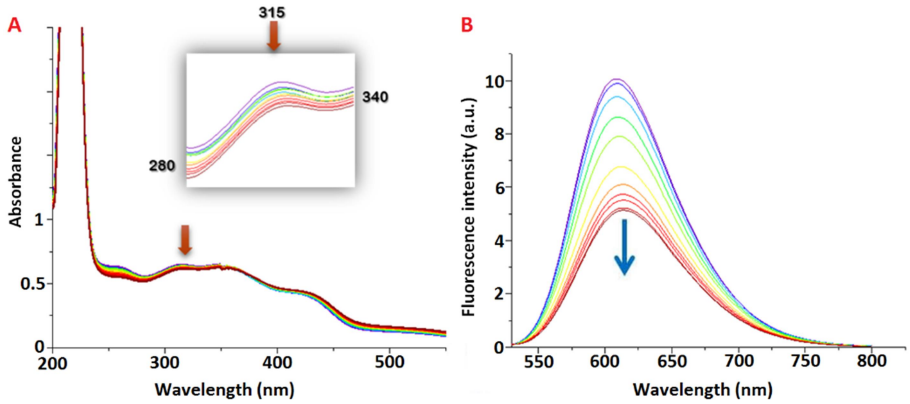

Figure S7. A) Absorption spectra of **R2** in 10 mM sodium cacodylate/20 mM NaCl buffer upon addition of ct-DNA (0−25 μM). The inset shows a zoom of the absorption region (MLCT band) used to determine the intrinsic binding constants K_b. B) Emission spectra of DNA–EB (obtained using [ct-DNA] = 25 μM and [EB] = 125 μM) in 10 mM sodium cacodylate, 20 mM NaCl, λ_{exc}= 514 nm, λ_{em}= 610 nm, upon addition of increasing amounts of R**2** (2.5–50 μM). The blue arrow shows the diminution of the emission intensity with the increase of complex concentration. The $[\text{ct-DNA}]_{bp}$ was determined from its absorption intensity at 260 nm, with a molar extinction coefficient of 6600 $M^{-1}cm^{-1}$ [3].

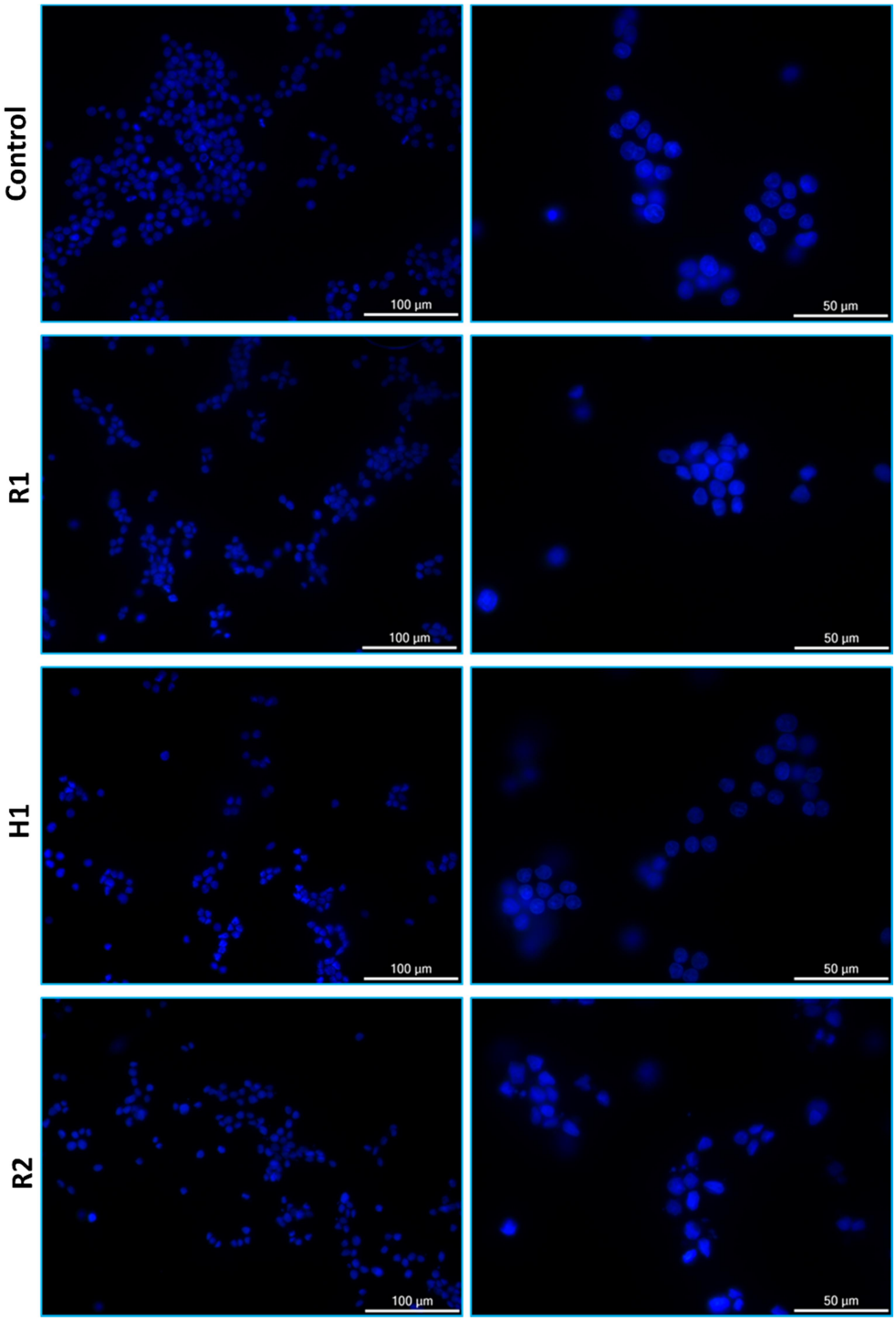

Figure S8. Confocal microscopy images showing the blue-stained nucleus of SW620 cells, SW620 cells incubated with **R1**, SW620 cells incubated with **H1** and SW620 cells incubated with **R2**. The concentrations of each compound used correspond to the corresponding IC_{50} values (see Table 2). The selected images are representative of three distinct series of images. Incubation time = 48 h; scale bars: left images, 100 µm and right images, 50 µm.

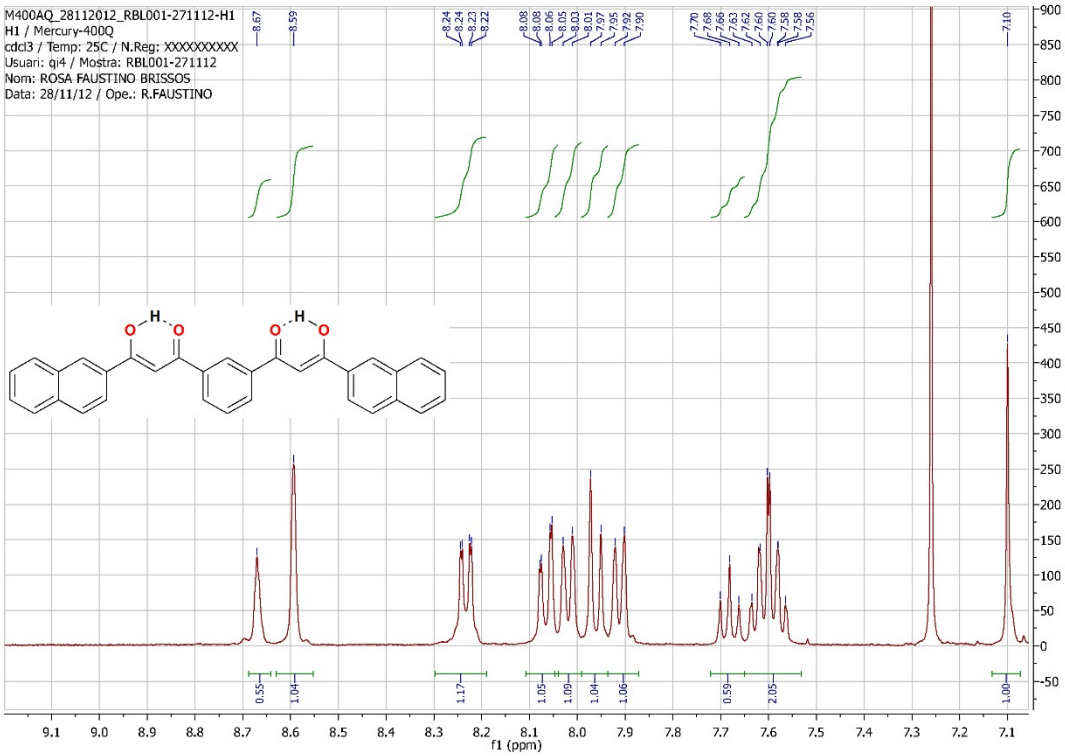

Figure S9. ^{1}H NMR spectrum of ligand **H_2L1** in $CDCl_3$. The enolic O−H proton is not seen (usually such acidic protons appear at δ > 15 ppm).

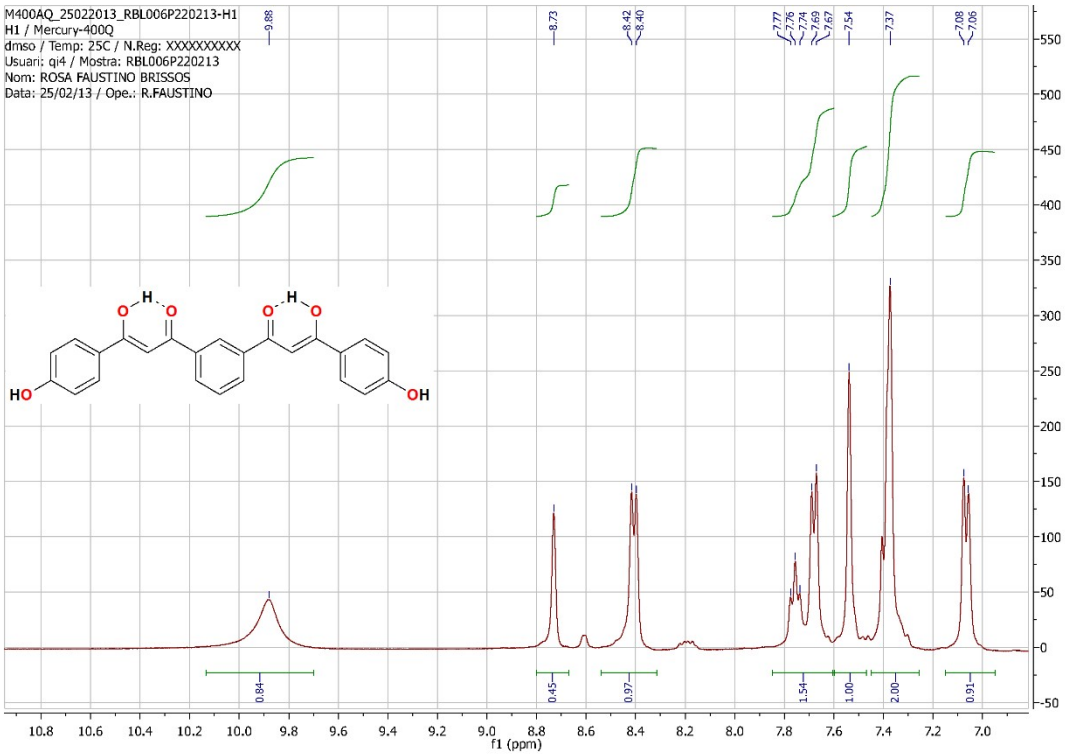

Figure S10. ^{1}H NMR spectrum of ligand **H_4L2** in d_6-DMSO. The enolic O−H proton is not seen (usually such acidic protons appear at δ > 15 ppm).

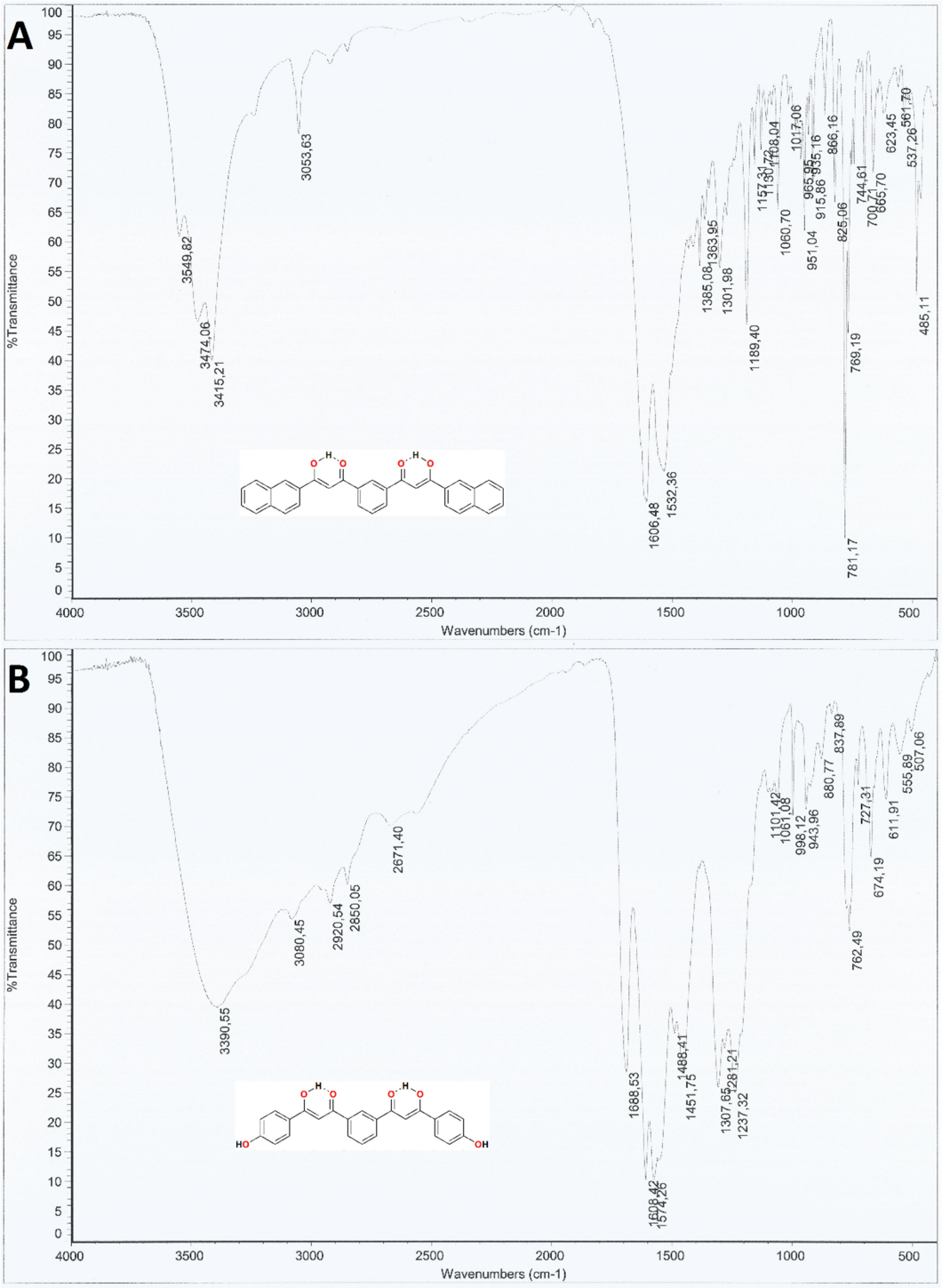

Figure S11. IR spectrum of A) ligand **H_2L1** and of B) ligand **H_4L2**.

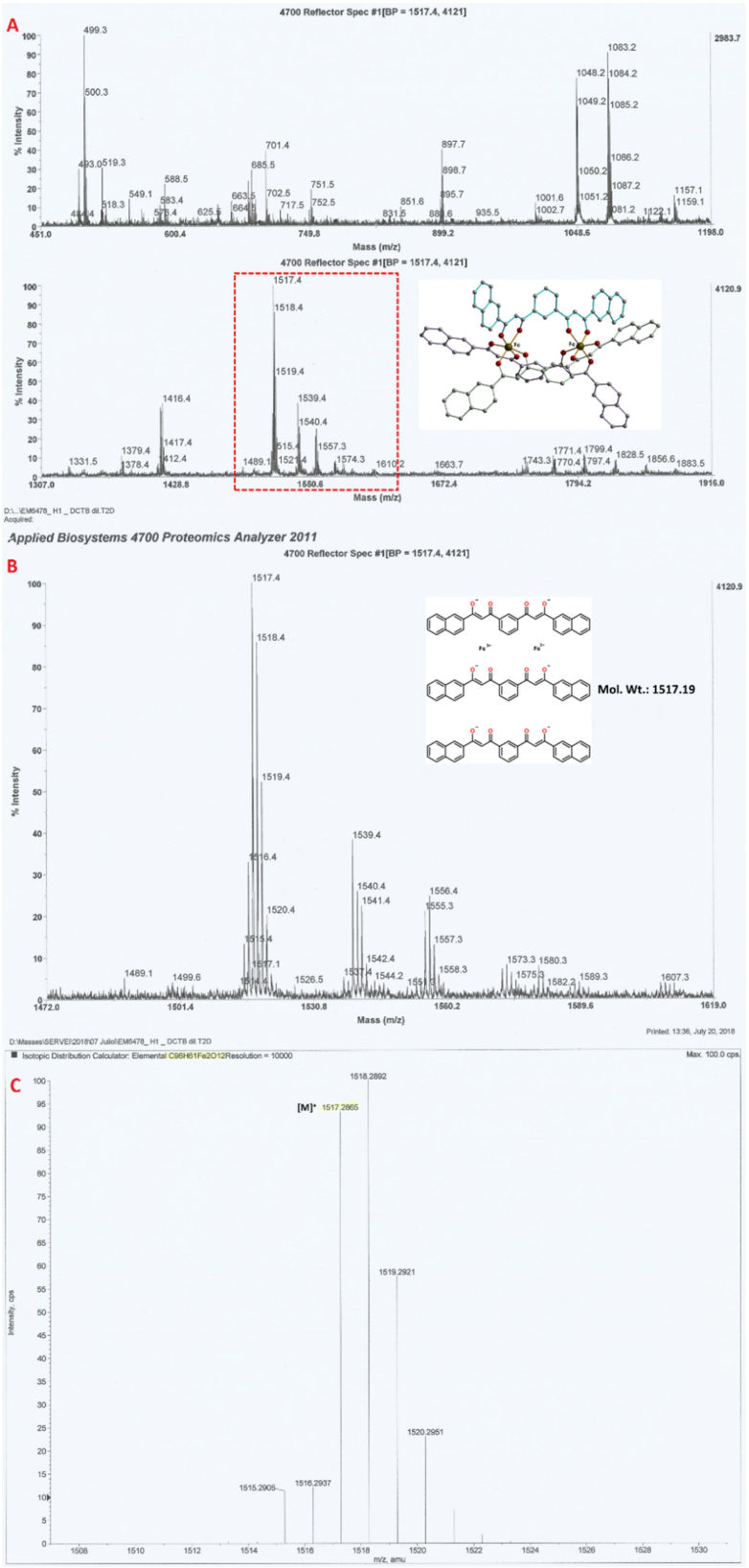

Figure S12. A) MALDI-TOF spectrum of **H1**; B) zoom of the Mol. Wt. region of the spectrum; C) theoretical isotopic pattern for the molecular peak of **H1**.

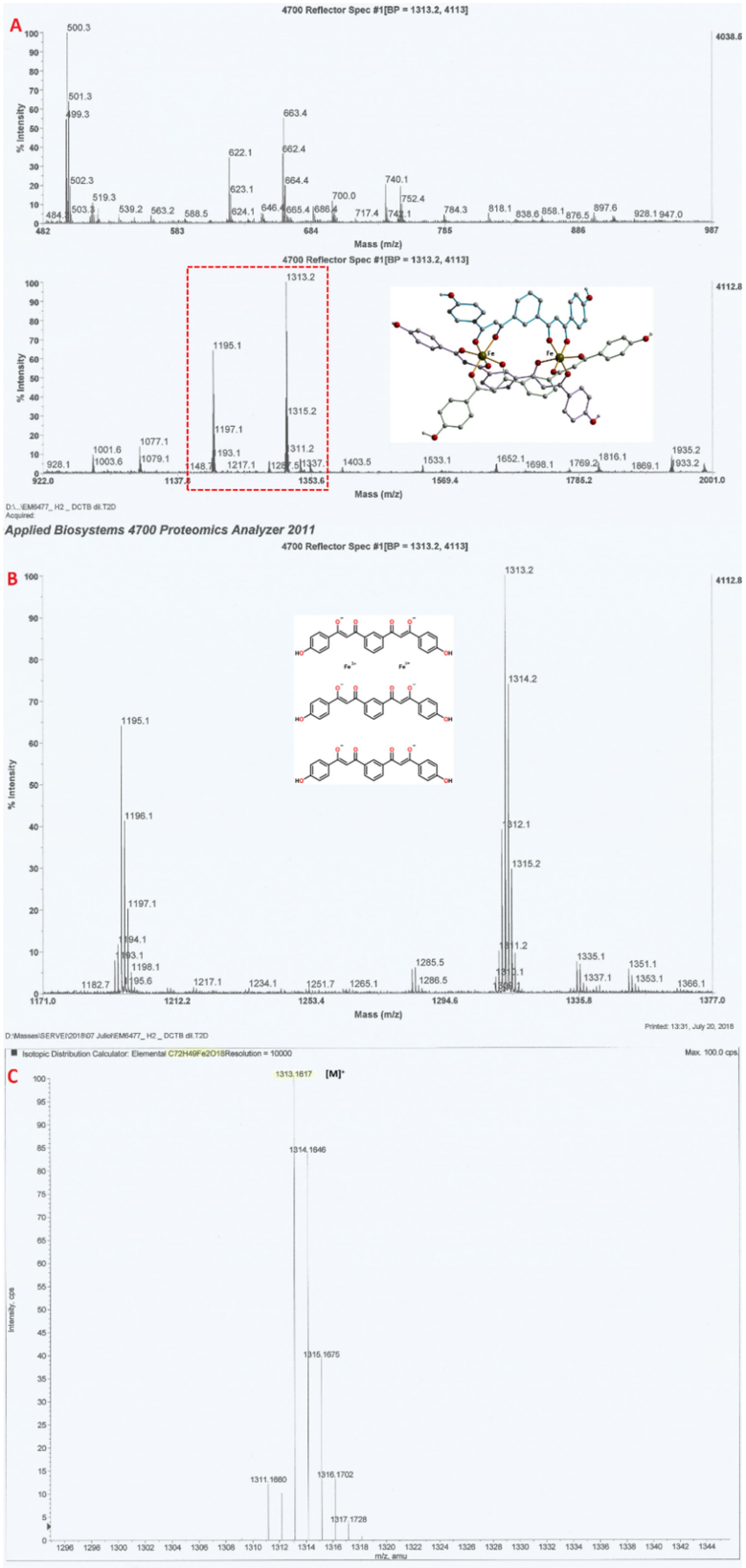

Figure S13. A) MALDI-TOF spectrum of **H2**; B) zoom of the Mol. Wt. region of the spectrum; C) theoretical isotopic pattern for the molecular peak of **H2**.

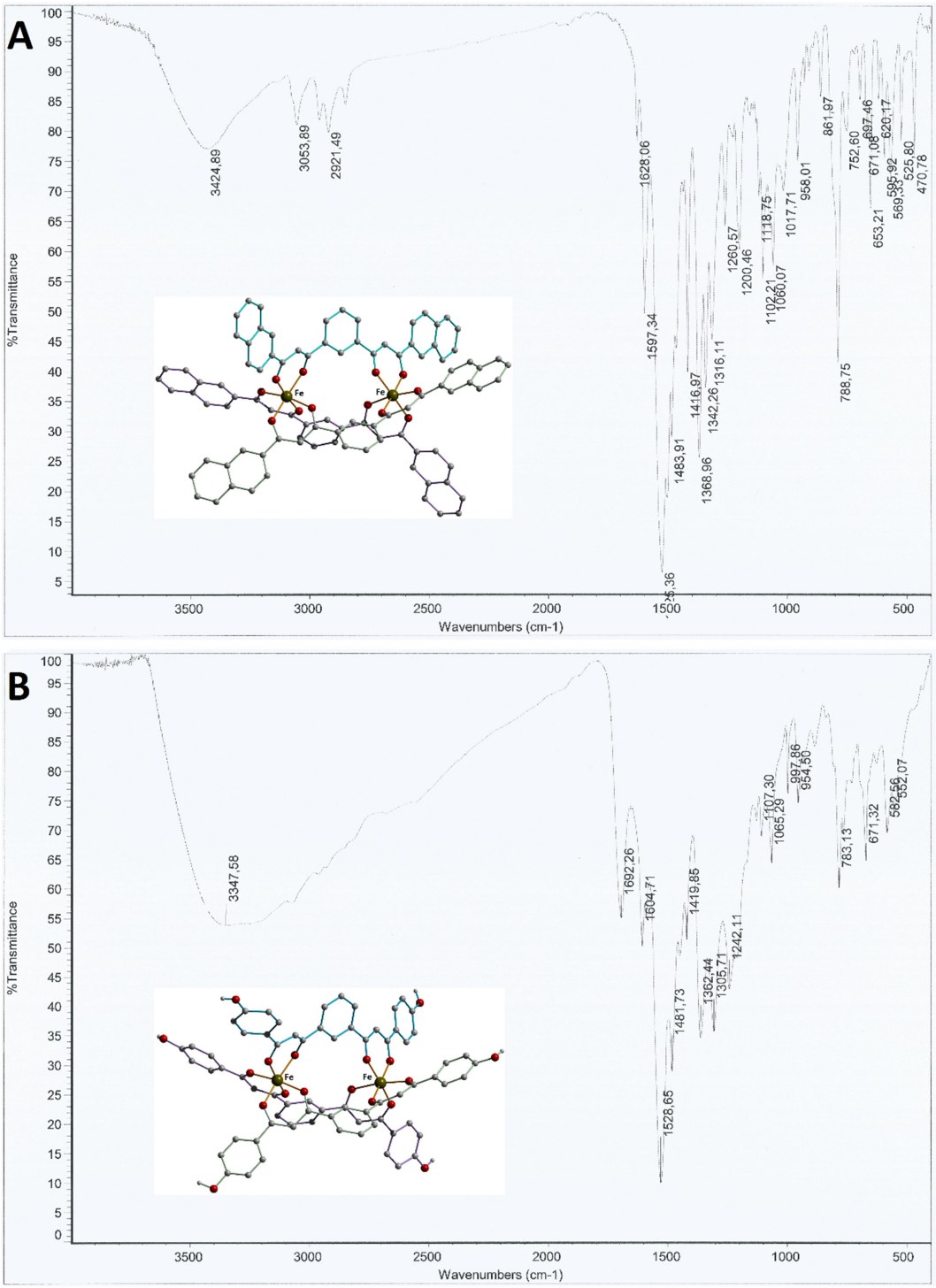

Figure S14. IR spectrum of A) helicate **H1** and of B) helicate **H2**.

References

[1] Meistermann I., Moreno V., Prieto M. J., Moldrheim E., Sletten E., Khalid S., Rodger P. M., Peberdy J. C., Isaac C. J., Rodger A., Hannon M. J., *Proc. Natl. Acad. Sci. U S A* **2002**, *99*, 5069-5074.

[2] Darawsheh M., Barrios L. A., Roubeau O., Teat S. J., Aromi G., *Chem.-Eur. J.* **2016**, *22*, 8635-8645.

[3] Reichmann M. E., Rice S. A., Thomas C. A., Doty P., *J. Am. Chem. Soc.* **1954**, *76*, 3047-3053.